

Article

Protonated Forms of Layered Perovskite-Like Titanate NaNdTiO_4 : Neutron and X-ray Diffraction Structural Analysis

Oleg I. Silyukov ^{*}, Sergey A. Kurnosenko , Iana A. Minich , Ivan A. Rodionov  and Irina A. Zvereva 

Department of Chemical Thermodynamics and Kinetics, Institute of Chemistry, Saint Petersburg State University, 198504 Saint Petersburg, Russia; st040572@student.spbu.ru (S.A.K.); st048953@student.spbu.ru (I.A.M.); i.rodionov@spbu.ru (I.A.R.); irina.zvereva@spbu.ru (I.A.Z.)

* Correspondence: oleg.silyukov@spbu.ru or olegsilyukov@yandex.ru

Abstract: Structures of partially and completely protonated Ruddlesden–Popper phases, $\text{H}_{0.7}\text{Na}_{0.3}\text{NdTiO}_4 \cdot 0.3\text{H}_2\text{O}$ and HNdTiO_4 , have been established by means of neutron and X-ray diffraction analysis and compared among themselves as well as with that of the initial titanate NaNdTiO_4 . It was shown that while interlayer sodium cations in the partially protonated form are coordinated by nine oxygen atoms, including one related to intercalated water, in the fully protonated compound the ninth oxygen proves to be an axial anion belonging to the opposite slab of titanium–oxygen octahedra. Moreover, the partially protonated titanate was found to significantly differ from the other two in the octahedron distortion pattern. It is characterized by a weakly pronounced elongation of the octahedra towards the Nd-containing interlayer space making Ti^{4+} cations practically equidistant from both axial oxygen atoms, which is accompanied by a low-frequency shift of the bands relating to the asymmetric stretching mode of axial Ti–O bonds observed in the Raman spectra.



Citation: Silyukov, O.I.; Kurnosenko, S.A.; Minich, I.A.; Rodionov, I.A.; Zvereva, I.A. Protonated Forms of Layered Perovskite-Like Titanate NaNdTiO_4 : Neutron and X-ray Diffraction Structural Analysis. *Solids* **2021**, *2*, 265–277. <https://doi.org/10.3390/solids2030017>

Academic Editor: Mirosław Mączka

Received: 20 April 2021

Accepted: 23 June 2021

Published: 1 July 2021

Publisher's Note: MDPI stays neutral with regard to jurisdictional claims in published maps and institutional affiliations.



Copyright: © 2021 by the authors. Licensee MDPI, Basel, Switzerland. This article is an open access article distributed under the terms and conditions of the Creative Commons Attribution (CC BY) license (<https://creativecommons.org/licenses/by/4.0/>).

Keywords: layered perovskite; titanate; protonation; hydration; structure; neutron diffraction

1. Introduction

Over past decades, great attention has been paid to ion-exchangeable layered perovskite-like oxides as promising ionic conductors [1–5], catalysts [6], photocatalysts [7–9], multipurpose precursors for the creation of hybrid inorganic–organic materials [10–18], nanoelectronic [19], ferroelectric [20], piezoelectric [21], luminescent [22] and photovoltaic devices [23], chemical sensors [24] as well as fuel cells [25].

Ion-exchangeable layered perovskites are crystalline solids possessing a block-type structure, which consists of negatively charged intergrowth slabs with a thickness of n corner-shared perovskite octahedra regularly alternating with interlayer spaces populated by alkali cations. Their valuable physical-chemical properties are associated with the unique perovskite structure as well as the pronounced activity of the interlayer space towards ion exchange and intercalation reactions [26,27]. In accordance with features of structure and composition, ion-exchangeable layered perovskites may be divided into two classes: Dion–Jacobson [28,29] and Ruddlesden–Popper phases [30,31]. The Dion–Jacobson phases follow a general formula $A'[A_{n-1}B_nO_{3n+1}]$, where A' is an alkali metal, A is alkaline earth or transition metal and B is Nb, Ta, Ti, Zr or related element. The relative arrangement of adjacent perovskite slabs in these compounds depends on the interlayer cation size. In particular, the Dion–Jacobson perovskites with comparatively small cations ($A' = \text{Li}, \text{Na}$) are usually characterized by a staggered conformation while in the case of larger ones ($A' = \text{K}, \text{Rb}, \text{Cs}$) an eclipsed conformation is more probable. Due to relatively low interlayer charge density, the Dion–Jacobson phases demonstrate high reactivity in a wide range of low-temperature transformations [32–35]. The structure of the Ruddlesden–Popper phases, described by a formula $A'_2[A_{n-1}B_nO_{3n+1}]$, represents alternation of perovskite slabs with the layers adopting the crystal arrangement of rock salt. These substances are characterized

by higher interlayer charge density and their adjacent perovskite slabs are usually stacked in a staggered conformation. The reactivity of the Ruddlesden–Popper perovskites is known to be lower in comparison with that of the Dion–Jacobson ones, although it appears to be enough for ion exchange and intercalation of small molecules via the soft chemistry approaches [36–41].

A deep understanding of the structural features of layered perovskite-like oxides is of great importance for the prediction of their physical-chemical properties and targeted research-based creation of materials with specified characteristics. For instance, ionic conductivity strongly depends on the equilibrium crystallographic positions of interlayer cations associated in turn with a degree of the perovskite octahedra distortion [42]. As well, the interlayer space is considered a separate reaction zone in heterogeneous photocatalysis providing superior photocatalytic activity of many layered perovskites in comparison with that of non-layered materials due to reversible reactants' intercalation [43]. In this regard, its structural features may significantly influence the supply of reactants and the withdrawal of products defining the reaction kinetics and, therefore, the photocatalyst performance. Moreover, the hydration degree and, apparently, crystallographic positions of intercalated water molecules affect the reactivity of layered perovskites with organic compounds [44]. Knowing these peculiarities greatly facilitates the creation of hybrid inorganic-organic materials for many promising applications.

Layered perovskite-like titanates $ALnTiO_4$ (A = alkali cation or proton, Ln = La or lanthanoid cation) are Ruddlesden–Popper phases whose unique structure is characterized by the complete ordering of the aforementioned cations between two nonequivalent interlayer spaces interbedded by perovskite slabs with a thickness of $n = 1$ titanium-oxygen octahedron experiencing pronounced vertical distortion [45,46]. These compounds attract the attention of researchers as promising proton conductors [47–51], catalysts [52], photocatalysts [53–56] as well as luminescent [57] and magnetically susceptible materials [58–60].

As shown in our previous reports [61,62], when placed in aqueous solutions, the alkaline titanates $ALnTiO_4$ undergo ion exchange and hydration giving protonated hydrated forms $H_xA_{1-x}LnTiO_4 \cdot yH_2O$ whose specific composition depends on the pH of the medium and a particular interlayer cation. Since many practically valuable processes, such as photocatalytic reactions, are conducted in aqueous media, a thorough investigation of water-stable forms of layered perovskites deserves special attention. In view of the foregoing, the present paper focuses on a structural study of two protonated forms of the layered perovskite-like titanate $NaNdTiO_4$, namely the partially protonated form $H_{0.7}Na_{0.3}NdTiO_4 \cdot 0.3H_2O$, existing in water excess, and the completely protonated one $HNdTiO_4$, being stable in acid media.

2. Materials and Methods

2.1. Synthesis

The alkaline layered perovskite-like titanate $NaNdTiO_4$ was synthesized according to the standard ceramic technique using preliminarily calcined TiO_2 , Nd_2O_3 and Na_2CO_3 as reactants. The oxides were taken in stoichiometric amounts, sodium carbonate—with a 30% excess to compensate for the loss during calcination. All the compounds were mixed and thoroughly ground in an agate mortar under a layer of n -hexane for 30 min per each gram. The mixture obtained was dried and pelletized into ~2 g tablets at 50 bar using an Omec PI 88.00 hydraulic press. The tablets were placed into corundum crucibles with lids, kept at 850 °C for 12 h in a Nabertherm L-011K2RN muffle furnace and, after cooling down, ground in an agate mortar.

To obtain the partially protonated hydrated form $H_{0.7}Na_{0.3}NdTiO_4 \cdot 0.3H_2O$, 1 g of $NaNdTiO_4$ was treated with 1000 mL of water at room temperature for 1 d. In the case of the completely protonated form $HNdTiO_4$ preparation, 1 g of $NaNdTiO_4$ was processed with 200 mL of a 0.1 M hydrochloric acid solution under the same conditions. Then the solid phases were separated from solutions via centrifuging and dried in a desiccator over CaO for 2 d.

2.2. Instrumentation

Powder X-ray diffraction (XRD) patterns of the samples were recorded on a Thermo Scientific ARL X'TRA diffractometer ($\text{CuK}\alpha$ radiation, angle range $2\theta = 5\text{--}120^\circ$, accumulation time 10 h). The lattice parameters calculation and Rietveld refinement were performed based on all the reflections observed using GSAS software. The initial structural parameters were adopted from the paper [63]. Neutron diffraction patterns were obtained on an IR-8 research neutron reactor (neutron wavelength $\lambda = 1.7526 \text{ \AA}$, angle range $2\theta = 10\text{--}130^\circ$, accumulation time 50 h). The samples were investigated in aluminum containers with a diameter of 3 mm and a wall thickness of 0.03 mm whose reduced diffraction peaks were subsequently subtracted from the patterns. The structure calculations were conducted using GSAS software. The initial parameters for the refinement were taken from the reports [63,64]. Thermogravimetric (TG) analysis was carried out on a Netzsch TG 209 F1 Libra thermobalance in an argon atmosphere. The temperature program included heating each sample from room temperature to 700°C at a rate of $10^\circ\text{C}/\text{min}$. The protonation degree and amount of intercalated water were determined according to the previously reported method [65]. Raman scattering spectra were collected on a Bruker Senterra spectrometer in the Raman shift range of $100\text{--}4000 \text{ cm}^{-1}$ using the incident laser 488 nm (power 20 mW , accumulation time 10 s). The high-frequency region in the figures was presented on an enlarged scale to make bands of water more visible relative to the high-intensity ones of the perovskite matrix.

3. Results and Discussion

Initial alkaline titanate NaNdTiO_4 and its protonated forms were identified using XRD analysis (Figure 1). Tetragonal lattice parameters of NaNdTiO_4 ($a = b = 3.75 \text{ \AA}$ $c = 12.82 \text{ \AA}$) and HNdTiO_4 ($a = b = 3.70 \text{ \AA}$ $c = 12.09 \text{ \AA}$) were found to be consistent with the literature values [46]. In the course of the partial protonation, the interlayer distance d is seen to increase (this is reflected in the shift of low-angle $00l$ reflections on the diffractogram to the region of lower values), which indicates probable water intercalation accompanying the ion exchange. Otherwise, the d value should have reduced since protons are much smaller than sodium cations. Moreover, the partially protonated form is amenable to indexing in another space group ($I4/mmm$ instead of $P4/nmm$) and is characterized by doubled c parameter, which is not observed in the case of NaNdTiO_4 and HNdTiO_4 . The space group change and the c parameter doubling appear to be caused by a probable transformation of the adjacent perovskite slabs conformation from staggered to eclipsed. The completely protonated titanate HNdTiO_4 , apparently, possesses the slabs arrangement similar to that of NaNdTiO_4 and does not contain a noticeable amount of interlayer water.

TG curves of the protonated samples are presented in Figure 2. In both cases, two main sections on the curves can be distinguished. The first of them corresponding to the temperatures up to 200°C refers to deintercalation of the interlayer water molecules resulting in the formation of an anhydrous partially or fully protonated titanate. At the second section ($250\text{--}650^\circ\text{C}$), the latter experiences topochemical dehydration consisting in the binding of the interlayer oxygen atoms and protons into water molecules, their liberation and closing vertices of titanium-oxygen octahedra of adjacent perovskite slabs. In this way, final thermolysis products follow a gross formula $\text{Na}_{1-x}\text{NdTiO}_{4-x/2}$, where x is the amount of protons in the initial compound. Processing of the curves allowed us to establish quantitative compositions signed in Figure 2. The partially protonated titanate contains a perceptible amount of intercalated water released during heating at low temperatures. It corresponds to the formula $\text{H}_{0.7}\text{Na}_{0.3}\text{NdTiO}_4 \cdot 0.3\text{H}_2\text{O}$ (specified $\text{H}_{0.73}\text{Na}_{0.27}\text{NdTiO}_4 \cdot 0.3\text{H}_2\text{O}$). The completely protonated HNdTiO_4 was found to exist in a practically anhydrous state.

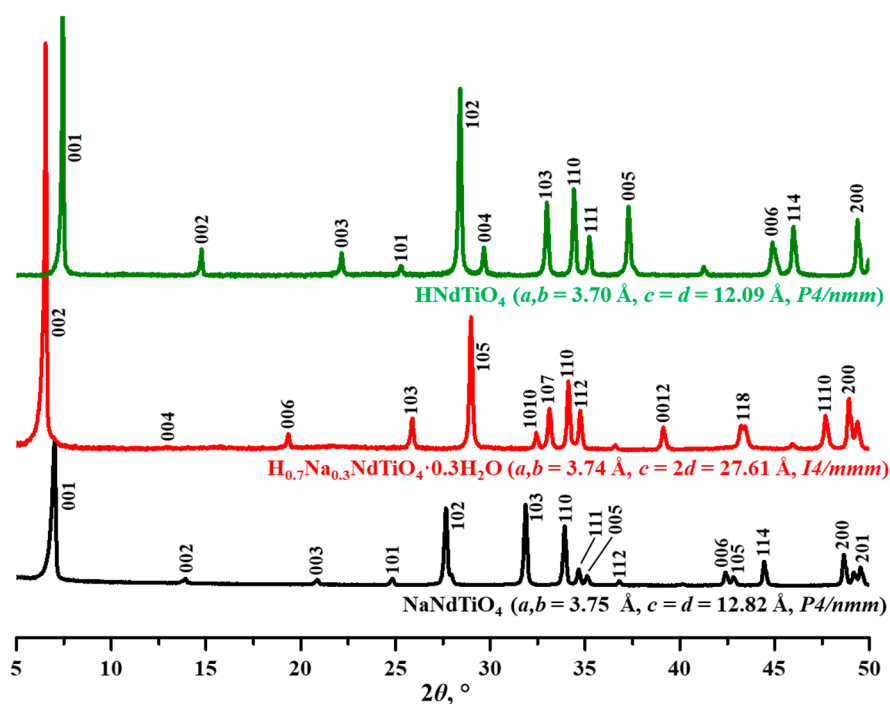


Figure 1. X-ray diffraction (XRD) patterns of the HNdTIO_4 , $\text{H}_{0.7}\text{Na}_{0.3}\text{NdTiO}_4 \cdot 0.3\text{H}_2\text{O}$ and NaNdTIO_4 samples.

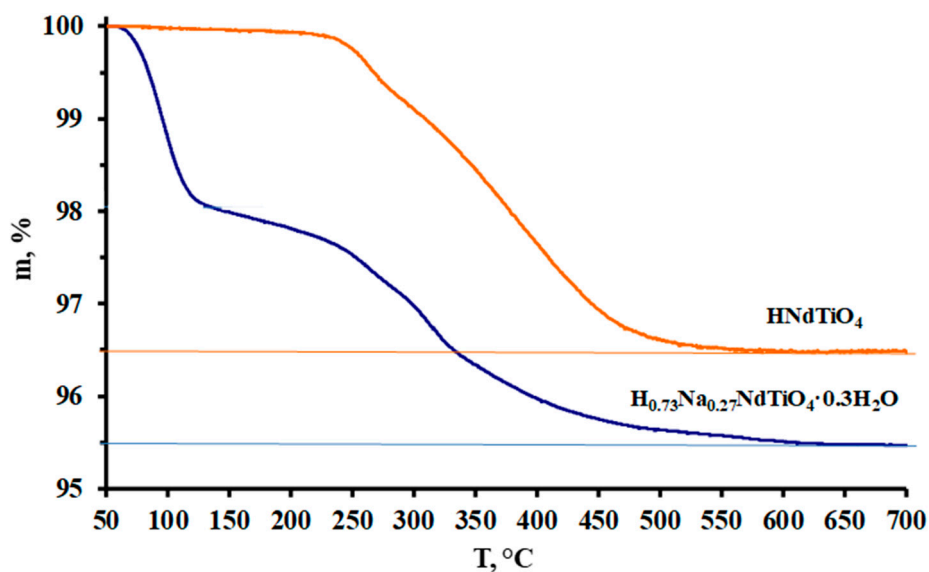


Figure 2. Thermogravimetric (TG) curves of partially and completely protonated samples.

The structural model of the partially protonated titanate $\text{H}_{0.7}\text{Na}_{0.3}\text{NdTiO}_4 \cdot 0.3\text{H}_2\text{O}$ was refined by the Rietveld method based on the XRD data (Figure 3) [62]. The XRD patterns collected made it possible to determine with high accuracy the positions of all the atoms constituting the compound, besides hydrogen (Table 1). All the parameters calculated fall in a physically reasonable range (although the Na occupancy factor and position are hardly reliable) and are consistent with the calculation data for the related La-containing titanate. Thus, the refinement of the $\text{H}_{0.7}\text{Na}_{0.3}\text{NdTiO}_4 \cdot 0.3\text{H}_2\text{O}$ structure can be considered successful.

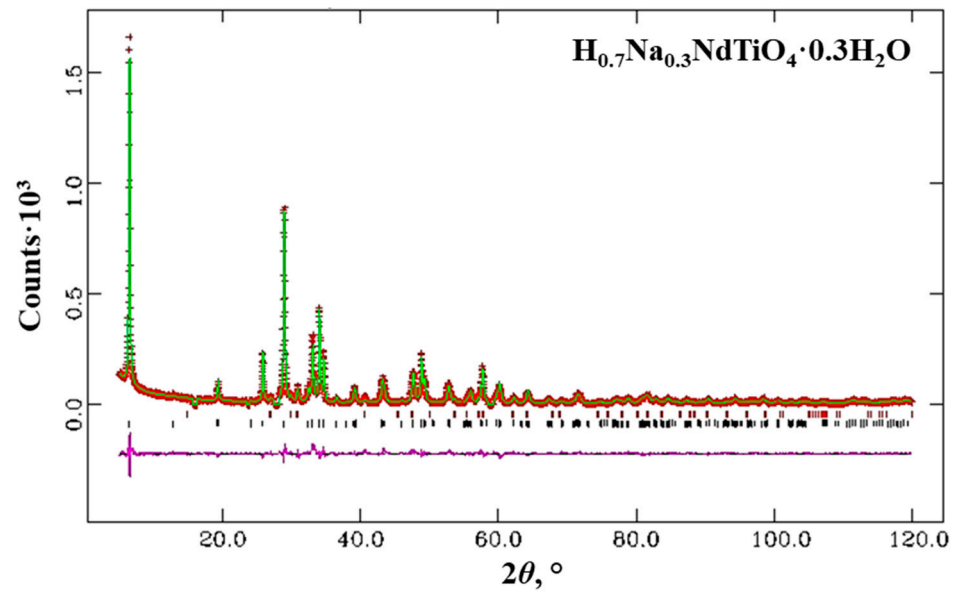


Figure 3. Experimental (red), calculated (green) and differential (purple) profiles of the $\text{H}_{0.7}\text{Na}_{0.3}\text{NdTiO}_4 \cdot 0.3\text{H}_2\text{O}$ XRD pattern.

Table 1. Results of the $\text{H}_{0.7}\text{Na}_{0.3}\text{NdTiO}_4 \cdot 0.3\text{H}_2\text{O}$ structure calculation based on XRD data.

$\text{H}_{0.7}\text{Na}_{0.3}\text{NdTiO}_4 \cdot 0.3\text{H}_2\text{O}$						
Tetragonal System, $I4/mmm$, $a = b = 3.7359 \text{ \AA}$, $c = 27.613 \text{ \AA}$, $R_{\text{wp}} = 0.1137$, $R(F^2) = 0.0854$						
Ion	Position	x	y	z	U_{iso}	Occupancy
Na	4e	0	0	0.4225 (25)	0.043 (10)	0.265 (14)
Nd	4e	0	0	0.30010 (7)	0.0006 (25)	1
Ti	4e	0	0	0.12489 (17)	0.004 (5)	1
O1	4e	0	0	0.0551 (7)	0.0036 (34)	1
O2	8g	0	0.5	0.13925 (34)	0.0084 (26)	1
O3	4e	0	0	0.2048 (9)	0.015 (4)	1
Ow	8j	0.388 (17)	0.5	0.0	0.025	0.314 (14)

An attempt to refine the neutron diffraction pattern was made for the fully protonated form (Figure 4). In accordance with the results obtained (Table 2), the determination of the HNdTiO_4 structure proved to be successful. All the parameters being refined take valid values and the difference between experimental and calculated profiles lies within the limits admissible for structural calculations.

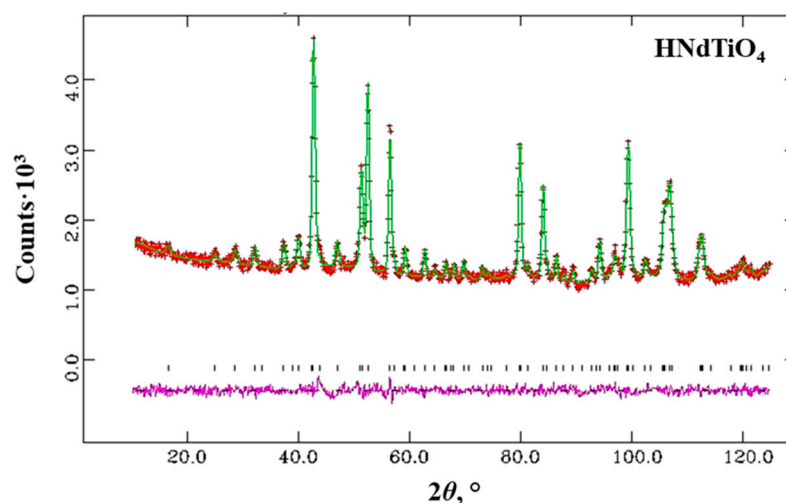


Figure 4. Experimental (red), calculated (green) and differential (purple) profiles of the HNdTlO₄ neutron diffraction pattern.

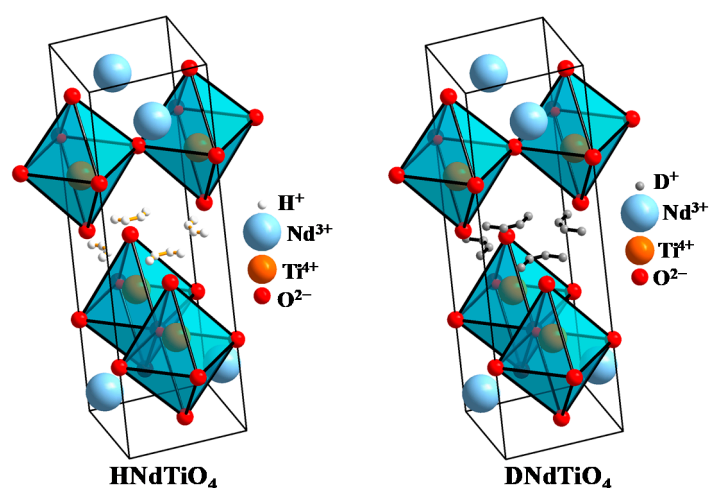
Table 2. Results of the HNdTlO₄ structure calculation based on neutron diffraction data.

HNdTlO ₄						
Tetragonal System, <i>P4/nmm</i> <i>a</i> = <i>b</i> = 3.6983 Å, <i>c</i> = 12.0928 Å, <i>R</i> _{wp} = 0.0253, <i>R</i> (<i>F</i> ²) = 0.0627						
Ion	Position	<i>x</i>	<i>y</i>	<i>z</i>	<i>U</i> _{iso}	Occupancy
H	16e	0.434 (12)	0.133 (12)	0.4966 (25)	0.045 (13)	0.125
Nd	2e	0.25	0.25	0.8834 (5)	0.0001 (13)	1
Ti	2e	0.25	0.25	0.2928 (8)	0.0152 (35)	1
O1	4g	0.25	0.75	0.2490 (5)	0.0093 (15)	1
O2	2e	0.25	0.25	0.0759 (6)	0.0093 (15)	1
O3	2e	0.25	0.25	0.4425 (8)	0.0177 (23)	1

Data on the comparison of HNdTlO₄, the structure of which was refined here, and its deuterated counterpart DNdTlO₄, the structure of which was refined in one of the earlier reports [64], are shown in Table 3 and Figure 5. Generally, the structural models of both compounds can be considered practically identical. The deuterated sample demonstrates a slightly greater lattice parameter in comparison with those of the non-deuterated one. In the latter protons are located closer to the axial oxygen that binds them than deuterium cations (0.919 Å vs. 0.932 Å). At the same time, the titanium–oxygen octahedron distortion is not proportional to the lattice parameter increasing. In particular, the bond Ti–O3 proves to be 0.01 Å longer in the deuterated titanate.

Table 3. Comparison of some bond lengths in HNdTiO₄ and DNdTiO₄ [64].

HNdTiO ₄		DNdTiO ₄	
Bond	Length, Å	Bond	Length, Å
H–O3 8x	0.919	D–O3 8x	0.932
Ti–O3 1x	1.810	Ti–O3 1x	1.789
Ti–O1 4x	1.923	Ti–O1 4x	1.919
Ti–O2 1x	2.623	Ti–O2 1x	2.633

**Figure 5.** Comparison of the HNdTiO₄ (this work) and DNdTiO₄ (data from [64]) structures. The equivalent positions of hydrogen and deuterium are connected by lines.

As noted earlier, the complete substitution of sodium cations by protons leads to a noticeable decrease of the distance between vertices of the ion-exchangeable layer octahedra. However, a space group change or a relative shift of adjacent slabs is not observed. In the case of the partially protonated hydrated titanate, the Rietveld refinement clearly confirms the relative shift of Nd-containing slabs by half of the *a* parameter along both horizontal axes accompanied by the space group change from *P4/nmm* to *I4/mmm*. In other words, water intercalation results not only in the interlayer space expansion, but also in the conformation change from staggered to eclipsed.

The graphical comparison of the partially protonated hydrated titanate H_{0.7}Na_{0.3}NdTiO₄·0.3H₂O investigated here and La-containing deuterated compound D_{0.34}Na_{0.66}LaTiO₄·0.59D₂O reported in [63] is presented in Figure 6. Both structures are practically identical. The distortion of titanium-oxygen octahedra in the form of elongation towards the ion-exchangeable interlayer space direction is hardly noticeable in the La-containing titanate. Equivalent positions of water molecules are significantly distant from each other. In the case of the Nd-containing compound, they are located almost at the same point directly between two sodium cations. In addition, the sodium cation is shifted towards the interlayer space, which is apparently due to the lower occupancy of equivalent water positions in the crystal.

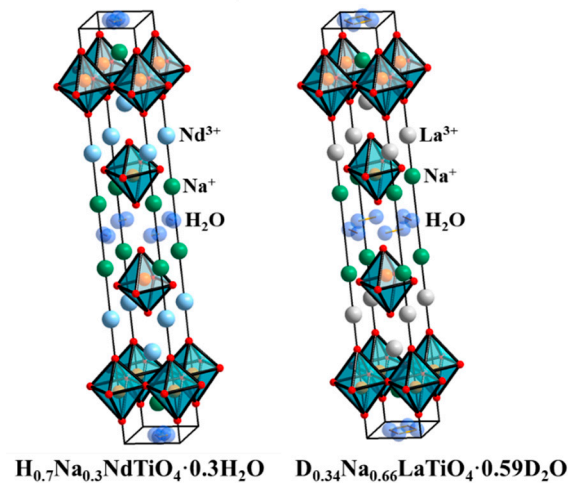


Figure 6. Comparison of the $\text{H}_{0.7}\text{Na}_{0.3}\text{NdTiO}_4 \cdot 0.3\text{H}_2\text{O}$ (this work) and $\text{D}_{0.34}\text{Na}_{0.66}\text{LaTiO}_4 \cdot 0.59\text{D}_2\text{O}$ (data from [63]) structures. Equivalent positions of water are connected by lines.

The sodium cations in $\text{H}_{0.7}\text{Na}_{0.3}\text{NdTiO}_4 \cdot 0.3\text{H}_2\text{O}$ are coordinated by nine oxygen atoms, including one belonging to the intercalated water similar to NaNdTiO_4 where the ninth oxygen is the axial anion of the opposite layer of the octahedra (Figure 7).

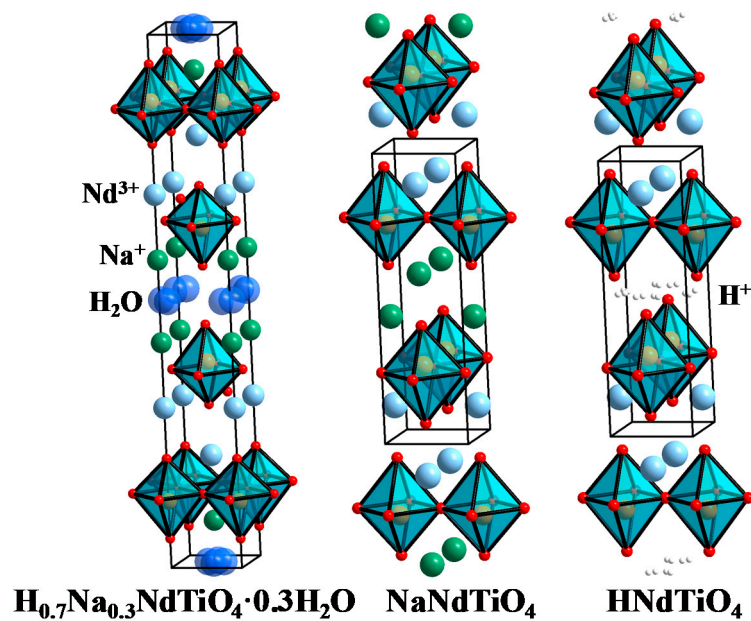


Figure 7. Comparison of the $\text{H}_{0.7}\text{Na}_{0.3}\text{NdTiO}_4 \cdot 0.3\text{H}_2\text{O}$ (this work), NaNdTiO_4 (data from [42]) and HNdTIO_4 (this work) structures.

An interesting fact found in this research is a change in the nature of the titanium-oxygen octahedron distortion in the partially protonated phase. The latter is different from NaNdTiO_4 and HNdTIO_4 in weak elongation of the octahedra towards the ion-exchangeable interlayer space, which allows the Ti^{4+} cation to be nearly equidistant from both axial oxygen atoms (Figure 8).



Figure 8. Titanium-oxygen octahedron geometry in the case of NaNdTiO_4 (data from [42]), HNdTiO_4 (this work) and $\text{H}_{0.7}\text{Na}_{0.3}\text{NdTiO}_4 \cdot 0.3\text{H}_2\text{O}$ (this work). The titanium-oxygen bond lengths are shown in the figure.

Raman spectra of the titanates under consideration are shown in Figure 9. The spectrum of the initial alkaline form NaNdTiO_4 is represented by the bands relating to symmetric (897 cm^{-1}) and asymmetric ($530, 620\text{ cm}^{-1}$) stretching modes of axial Ti–O bonds as well as to the vibrations located in the $(\text{NdO})_2$ layer ($280\text{--}330\text{ cm}^{-1}$) and in the Na-containing interlayer space ($100\text{--}200\text{ cm}^{-1}$). The formation of the partially protonated hydrated derivative $\text{H}_{0.7}\text{Na}_{0.3}\text{NdTiO}_4 \cdot 0.3\text{H}_2\text{O}$ is accompanied by the appearance of characteristic bands referred to the latitudinal vibrations ($1620\text{--}1630\text{ cm}^{-1}$) and stretching ($2800\text{--}3650\text{ cm}^{-1}$) of the interlayer water. Width and inhomogeneity of the latter point at the unequal involvement of the water molecules in the formation of hydrogen bonds with the titanate. Furthermore, partial protonation leads to the splitting of the symmetric stretching mode of axial Ti–O bonds into two bands (785 and 897 cm^{-1}) confirming the existence of two types of titanium-oxygen octahedra with unequal axial Ti–O distances, whose interlayer vertices are bonded to protons or hydroxonium ions ($\text{Ti-O}^- \text{H}^+$ or $\text{Ti-O}^- \text{H}_3\text{O}^+$, the first band) and sodium cations ($\text{Ti-O}^- \text{Na}^+$, the second band). The frequencies of the $(\text{NdO})_2$ vibrations are seen to reduce (265 and 305 cm^{-1}) due to the pronounced octahedron distortion. Protonation also results in numerous changes in the low-frequency spectral region ($100\text{--}200\text{ cm}^{-1}$) reflecting changes in the interlayer space composition. In the case of the completely protonated compound HNdTiO_4 , the bands of water vibrations are significantly less intense in comparison with those for $\text{H}_{0.7}\text{Na}_{0.3}\text{NdTiO}_4 \cdot 0.3\text{H}_2\text{O}$. Thus, HNdTiO_4 contains trace water amounts, which is fully consistent with the behavior of its TG curve. The band of the symmetric stretching mode of axial Ti–O bonds occupies a more low-frequency position (835 cm^{-1}) than in the alkaline titanate (897 cm^{-1}), which may be due to the more covalent nature of the $\text{O}^- \text{H}^+$ bond and, consequently, greater axial Ti–O distance. At the same time, the frequencies of asymmetric stretching modes of axial Ti–O bonds ($545, 610\text{ cm}^{-1}$) and vibrations of the $(\text{NdO})_2$ layer ($280\text{--}330\text{ cm}^{-1}$) prove to be close to those for NaNdTiO_4 . Consequently, the octahedra in HNdTiO_4 are significantly less distorted than in $\text{H}_{0.7}\text{Na}_{0.3}\text{NdTiO}_4 \cdot 0.3\text{H}_2\text{O}$, which is consistent with the structural analysis data.

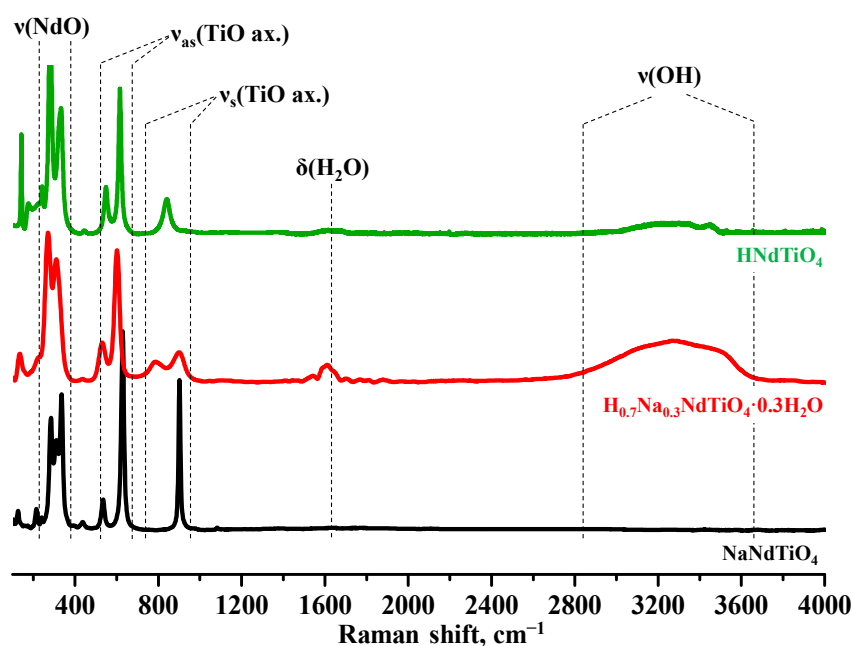


Figure 9. Raman spectra of the HNdTiO_4 , $\text{H}_{0.7}\text{Na}_{0.3}\text{NdTiO}_4 \cdot 0.3\text{H}_2\text{O}$ and NaNdTiO_4 samples.

4. Conclusions

In the present research, structures of partially and completely protonated Ruddlesden–Popper titanates, namely $\text{H}_{0.7}\text{Na}_{0.3}\text{NdTiO}_4 \cdot 0.3\text{H}_2\text{O}$ and HNdTiO_4 , have been refined by the Rietveld method on the basis of neutron and X-ray diffraction analysis and compared among themselves as well as with that of the initial alkaline compound NaNdTiO_4 . It was demonstrated that while interlayer sodium cations in the partially protonated titanate are coordinated by nine oxygen atoms, including one from the intercalated water, in the fully protonated compound the ninth oxygen is the axial anion belonging to the opposite slab of titanium–oxygen octahedra. Furthermore, the partially protonated titanate was revealed to significantly differ from the other two in the octahedron distortion pattern. The compound is characterized by weakly pronounced elongation of the octahedra towards the Nd-containing interlayer space making Ti^{4+} cations practically equidistant from both axial oxygen atoms, which is accompanied by a low-frequency shift of the bands relating to the asymmetric stretching mode of axial Ti–O bonds observed in the Raman spectra.

Author Contributions: Conceptualization, O.I.S., methodology, O.I.S. and I.A.Z.; investigation, O.I.S., S.A.K. and I.A.M.; data curation, O.I.S.; writing—original draft preparation, O.I.S. and S.A.K.; writing—review and editing, O.I.S. and I.A.R.; visualization, O.I.S. and S.A.K.; supervision, I.A.Z.; funding acquisition, O.I.S. and I.A.Z. All authors have read and agreed to the published version of the manuscript.

Funding: The study was financially supported by Russian Science Foundation (project No. 20-73-00027).

Data Availability Statement: The data presented in this study are available in the article.

Acknowledgments: The study was conducted using the equipment of the National Research Centre «Kurchatov Institute» and the Saint Petersburg State University Research Park: Centre for X-ray Diffraction Studies, Centre for Thermal Analysis and Calorimetry, Centre for Optical and Laser Research.

Conflicts of Interest: The authors declare no conflict of interest.

References

1. Thangadurai, V.; Shukla, A.; Gopalakrishnan, J. Proton conduction in layered perovskite oxides. *Solid State Ion.* **1994**, *73*, 9–14. [[CrossRef](#)]
2. Toda, K.; Watanabe, J.; Satoh, M. Synthesis and ionic conductivity of new layered perovskite compound, $\text{Ag}_2\text{La}_2\text{Ti}_3\text{O}_{10}$. *Solid State Ion.* **1996**, *90*, 15–19. [[CrossRef](#)]
3. Sato, M.; Abo, J.; Jin, T.; Ohta, M. Structure and ionic conductivity of MLaNb_2O_7 (M-K, Na, Li, H). *J. Alloys Compd.* **1993**, *192*, 81–83. [[CrossRef](#)]
4. Toda, K.; Suzuki, T.; Sato, M. Synthesis and high ionic conductivity of new layered perovskite compounds, $\text{AgLaTa}_2\text{O}_7$ and $\text{AgCa}_2\text{Ta}_3\text{O}_{10}$. *Solid State Ion.* **1997**, *93*, 177–181. [[CrossRef](#)]
5. Sato, M.; Watanabe, J.; Kazuyoshi, U. Crystal Structure and Ionic Conductivity of a Layered-Perovskite $\text{AgLaNb}_2\text{O}_7$. *J. Solid State Chem.* **1993**, *107*, 460–470. [[CrossRef](#)]
6. Campbell, K.D. Layered and double perovskites as methane coupling catalysts. *Catal. Today* **1992**, *13*, 245–253. [[CrossRef](#)]
7. Rodionov, I.A.; Zvereva, I.A. Photocatalytic activity of layered perovskite-like oxides in practically valuable chemical reactions. *Russ. Chem. Rev.* **2016**, *85*, 248–279. [[CrossRef](#)]
8. Hinterding, R.; Feldhoff, A. Two-Dimensional Oxides: Recent Progress in Nanosheets. *Z. Phys. Chem.* **2018**, *233*, 117–165. [[CrossRef](#)]
9. Hu, Y.; Mao, L.; Guan, X.; Tucker, K.A.; Xie, H.; Wu, X.; Shi, J. Layered perovskite oxides and their derivative nanosheets adopting different modification strategies towards better photocatalytic performance of water splitting. *Renew. Sustain. Energy Rev.* **2020**, *119*, 109527. [[CrossRef](#)]
10. Tahara, S.; Ichikawa, T.; Kajiwara, G.; Sugahara, Y. Reactivity of the Ruddlesden–Popper Phase $\text{H}_2\text{La}_2\text{Ti}_3\text{O}_{10}$ with Organic Compounds: Intercalation and Grafting Reactions. *Chem. Mater.* **2007**, *19*, 2352–2358. [[CrossRef](#)]
11. Minich, I.A.; Silyukov, O.I.; Gak, V.V.; Borisov, E.V.; Zvereva, I.A. Synthesis of Organic–Inorganic Hybrids Based on Perovskite-like Bismuth Titanate $\text{H}_2\text{K}_{0.5}\text{Bi}_{2.5}\text{Ti}_4\text{O}_{13}\cdot\text{H}_2\text{O}$ and n-Alkylamines. *ACS Omega* **2020**, *5*, 8158–8168. [[CrossRef](#)] [[PubMed](#)]
12. Silyukov, O.I.; Kurnosenko, S.A.; Zvereva, I.A. Intercalation of Methylamine into the Protonated Forms of Layered Perovskite-Like Oxides HLnTiO_4 (Ln = La and Nd). *Glas. Phys. Chem.* **2018**, *44*, 428–432. [[CrossRef](#)]
13. Kurnosenko, S.A.; Silyukov, O.I.; Mazur, A.S.; Zvereva, I.A. Synthesis and thermal stability of new inorganic-organic perovskite-like hybrids based on layered titanates HLnTiO_4 (Ln = La, Nd). *Ceram. Int.* **2020**, *46*, 5058–5068. [[CrossRef](#)]
14. Shelyapina, M.G.; Lushpinskaya, I.P.; Kurnosenko, S.A.; Silyukov, O.I.; Zvereva, I.A. Identification of Intercalates and Grafted Organic Derivatives of $\text{H}_2\text{La}_2\text{Ti}_3\text{O}_{10}$ by Multinuclear NMR. *Russ. J. Gen. Chem.* **2020**, *90*, 760–761. [[CrossRef](#)]
15. Kurnosenko, S.A.; Silyukov, O.I.; Minich, I.A.; Zvereva, I.A. Exfoliation of methylamine and n-butylamine derivatives of layered perovskite-like oxides HLnTiO_4 and $\text{H}_2\text{Ln}_2\text{Ti}_3\text{O}_{10}$ (Ln = La, Nd) into nanolayers. *Russ. J. Gen. Chem.* **2020**, *44*, 428–432.
16. Rodionov, I.A.; Maksimova, E.A.; Pozhidaev, A.Y.; Kurnosenko, S.A.; Silyukov, O.I.; Zvereva, I.A. Layered Titanate $\text{H}_2\text{Nd}_2\text{Ti}_3\text{O}_{10}$ Intercalated with n-Butylamine: A New Highly Efficient Hybrid Photocatalyst for Hydrogen Production from Aqueous Solutions of Alcohols. *Front. Chem.* **2019**, *7*, 863. [[CrossRef](#)] [[PubMed](#)]
17. Voytovich, V.V.; Kurnosenko, S.A.; Silyukov, O.I.; Rodionov, I.A.; Minich, I.A.; Zvereva, I.A. Study of n-alkylamine Intercalated Layered Perovskite-Like Niobates $\text{HCa}_2\text{Nb}_3\text{O}_{10}$ as Photocatalysts for Hydrogen Production from an Aqueous Solution of Methanol. *Front. Chem.* **2020**, *8*, 300. [[CrossRef](#)]
18. Shelyapina, M.G.; Silyukov, O.I.; Lushpinskaya, I.P.; Kurnosenko, S.A.; Mazur, A.S.; Shenderovich, I.G.; Zvereva, I.A. NMR Study of Intercalates and Grafted Organic Derivatives of $\text{H}_2\text{La}_2\text{Ti}_3\text{O}_{10}$. *Molecules* **2020**, *25*, 5229. [[CrossRef](#)]
19. Osada, M.; Sasaki, T. Exfoliated oxide nanosheets: New solution to nanoelectronics. *J. Mater. Chem.* **2009**, *19*, 2503–2511. [[CrossRef](#)]
20. Peláiz-Barranco, A.; González-Abreu, Y. Ferroelectric ceramic materials of the Aurivillius family. *J. Adv. Dielectr.* **2013**, *3*, 1330003. [[CrossRef](#)]
21. Moure, A. Review and perspectives of Aurivillius structures as a lead-free Piezoelectric system. *Appl. Sci.* **2018**, *8*, 62. [[CrossRef](#)]
22. Ida, S.; Ogata, C.; Eguchi, M.; Youngblood, W.J.; Mallouk, T.E.; Matsumoto, Y. Photoluminescence of perovskite nanosheets prepared by exfoliation of layered oxides, $\text{K}_2\text{Ln}_2\text{Ti}_3\text{O}_{10}$, KLnNb_2O_7 , and $\text{RbLnTa}_2\text{O}_7$ (Ln: Lanthanide ion). *J. Am. Chem. Soc.* **2008**, *130*, 7052–7059. [[CrossRef](#)] [[PubMed](#)]
23. Bi, D.; Tress, W.; Dar, M.I.; Gao, P.; Luo, J.; Renevier, C.; Schenk, K.; Abate, A.; Giordano, F.; Baena, J.C.; et al. Efficient luminescent solar cells based on tailored mixed-cation perovskites. *Sci. Adv.* **2016**, *2*, e1501170. [[CrossRef](#)] [[PubMed](#)]
24. Szczepanski, F.; Bayart, A.; Katelnikovas, A.; Blach, J.F.; Rousseau, J.; Saitzek, S. Luminescence and up-conversion properties in $\text{La}_2\text{Ti}_2\text{O}_7\cdot\text{Eu}^{3+},\text{Er}^{3+}$ oxides under UV and NIR radiations towards a two-color sensor. *J. Alloys Compd.* **2020**, *826*, 154157. [[CrossRef](#)]
25. Yuan, M.; Dong, W.; Wei, L.; Liu, Q.; Meng, Y.; Wang, X.; Wang, B.; Zhu, B. Stability study of SOFC using layered perovskite oxide $\text{La}_{1.85}\text{Sr}_{0.15}\text{CuO}_4$ mixed with ionic conductor as membrane. *Electrochim. Acta* **2020**, *332*, 135487. [[CrossRef](#)]
26. Schaak, R.E.; Mallouk, T.E. Perovskites by Design: A Toolbox of Solid-State Reactions. *Chem. Mater.* **2002**, *14*, 1455–1471. [[CrossRef](#)]
27. Uppuluri, R.; Sen Gupta, A.; Rosas, A.S.; Mallouk, T.E. Soft chemistry of ion-exchangeable layered metal oxides. *Chem. Soc. Rev.* **2018**, *47*, 2401–2430. [[CrossRef](#)] [[PubMed](#)]
28. Dion, M.; Ganne, M.; Tournoux, M. Nouvelles familles de phases $\text{M}^{\text{I}}\text{M}^{\text{II}}_2\text{Nb}_3\text{O}_{10}$ a feuilletés “perovskites”. *Mater. Res. Bull.* **1981**, *16*, 1429–1435. [[CrossRef](#)]

29. Jacobson, A.J.; Johnson, J.W.; Lewandowski, J.T. Interlayer Chemistry between Thick Transition-Metal Oxide Layers: Synthesis and Intercalation Reactions of $K[Ca_2Na_{n-3}Nb_nO_{3n+1}]$ ($3 \leq n \leq 7$). *Inorg. Chem.* **1985**, *24*, 3727–3729. [[CrossRef](#)]
30. Gopalakrishnan, J.; Bhat, V. $A_2Ln_2Ti_3O_{10}$ ($A =$ potassium or rubidium; $Ln =$ lanthanum or rare earth): A new series of layered perovskites exhibiting ion exchange. *Inorg. Chem.* **1987**, *26*, 4299–4301. [[CrossRef](#)]
31. Gopalakrishnan, J.; Sivakumar, T.; Ramesha, K.; Thangadurai, V.; Subbanna, G.N. Transformations of Ruddlesden–Popper Oxides to New Layered Perovskite Oxides by Metathesis Reactions. *Chem. Phys.* **2000**, *122*, 6237–6241. [[CrossRef](#)]
32. Jacobson, A.J.; Lewandowski, J.T.; Johnson, J.W. Ion exchange of the layered perovskite $KCa_2Nb_3O_{10}$ by protons. *J. Less Common Met.* **1986**, *116*, 137–146. [[CrossRef](#)]
33. Jacobson, A.J.; Johnson, J.W.; Lewandowski, J. Intercalation of the layered solid acid $HCa_2Nb_3O_{10}$ by organic amines. *Mater. Res. Bull.* **1987**, *22*, 45–51. [[CrossRef](#)]
34. Tahara, S.; Sugahara, Y. Interlayer Surface Modification of the Protonated Triple-Layered Perovskite $HCa_2Nb_3O_{10} \cdot xH_2O$ with n -Alcohols. *Langmuir* **2003**, *19*, 9473–9478. [[CrossRef](#)]
35. Yafarova, L.V.; Silyukov, O.I.; Myshkovskaya, T.D.; Minich, I.A.; Zvereva, I.A. New data on protonation and hydration of perovskite-type layered oxide $KCa_2Nb_3O_{10}$. *J. Therm. Anal. Calorim.* **2020**. [[CrossRef](#)]
36. Rodionov, I.A.; Silyukov, O.I.; Utkina, T.D.; Chislov, M.V.; Sokolova, Y.P.; Zvereva, I.A. Photocatalytic properties and hydration of perovskite-type layered titanates $A_2Ln_2Ti_3O_{10}$ ($A = Li, Na, K; Ln = La, Nd$). *Russ. J. Gen. Chem.* **2012**, *82*, 1191–1196. [[CrossRef](#)]
37. Rodionov, I.A.; Mechtaeva, E.V.; Burovikhina, A.A.; Silyukov, O.I.; Toikka, M.A.; Zvereva, I.A. Effect of protonation on the photocatalytic activity of the $K_2La_2Ti_3O_{10}$ layered oxide in the reaction of hydrogen production. *Mon. Chem. Chem. Mon.* **2018**, *149*, 475–482. [[CrossRef](#)]
38. Rodionov, I.A.; Fateev, S.A.; Zvereva, I.A. Synthesis of a New Layered $Rb_2Nd_2Ti_3O_{10}$ Oxide, Its Hydration and Protonation. *Glas. Phys. Chem.* **2017**, *43*, 593–596. [[CrossRef](#)]
39. Rodionov, I.A.; Sokolova, I.P.; Silyukov, O.I.; Burovikhina, A.A.; Fateev, S.A.; Zvereva, I.A. Protonation and Photocatalytic Activity of the $Rb_2La_2Ti_3O_{10}$ Layered Oxide in the Reaction of Hydrogen Production. *Int. J. Photoenergy* **2017**, *2017*, 9628146. [[CrossRef](#)]
40. Silyukov, O.I.; Minich, I.A.; Zvereva, I.A. Synthesis of Protonated Derivatives of Layered Perovskite-Like Bismuth Titanates. *Glas. Phys. Chem.* **2018**, *44*, 115–119. [[CrossRef](#)]
41. Kurnosenko, S.A.; Silyukov, O.I.; Zvereva, I.A. Preparation of Porous Particles of Layered Perovskite-Like Titanate $HLnTiO_4$. *Glas. Phys. Chem.* **2020**, *46*, 272–276. [[CrossRef](#)]
42. Byeon, S.; Kileung, P.; Park, K. Structure and Ionic Conductivity of $NaLnTiO_4$, Comparison with Those of $Na_2Ln_2Ti_3O_{10}$ ($Ln = La, Nd, Sm, \text{ and } Gd$). *J. Solid State Chem.* **1996**, *121*, 430–436. [[CrossRef](#)]
43. Cui, W.; Liu, L.; Ma, S.; Liang, Y.; Zhang, Z. CdS-sensitized $K_2La_2Ti_3O_{10}$ composite: A new photocatalyst for hydrogen evolution under visible light irradiation. *Catal. Today* **2013**, *207*, 44–49. [[CrossRef](#)]
44. Takahashi, S.; Nakato, T.; Hayashi, S.; Sugahara, Y.; Kuroda, K. Formation of Methoxy-Modified Interlayer Surface via the Reaction between Methanol and Layered Perovskite $HLnNb_2O_7 \cdot cntdot \cdot xH_2O$. *Inorg. Chem.* **1995**, *34*, 5065–5069. [[CrossRef](#)]
45. Blasse, G. Crystallographic data of sodium lanthanide titanates ($NaLnTiO_4$). *J. Inorg. Nucl. Chem.* **1968**, *30*, 656–658. [[CrossRef](#)]
46. Byeon, S.; Yoon, J.J.; Lee, S.O. A New Family of Protonated Oxides $HLnTiO_4$ ($Ln = La, Nd, Sm, \text{ and } Gd$). *J. Solid State Chem.* **1996**, *127*, 119–122. [[CrossRef](#)]
47. Pradhan, D.K.; Samantaray, B.K.; Choudhary, R.N.; Thakur, A.K. Complex impedance studies on a layered perovskite ceramic oxide— $NaNdTiO_4$. *Mater. Sci. Eng. B* **2005**, *116*, 7–13. [[CrossRef](#)]
48. Pradhan, D.K.; Samantaray, B.K.; Choudhary, R.N.; Thakur, A.K. Complex impedance analysis of $NaLaTiO_4$ electroceramics. *J. Mater. Sci. Mater. Electron.* **2006**, *17*, 157–164. [[CrossRef](#)]
49. Petrov, A.A.; Melnikova, N.A.; Petrov, A.V.; Silyukov, O.I.; Murin, I.V.; Zvereva, I.A. Experimental investigation and modelling of the Na^+ mobility in $NaLnTiO_4$ ($Ln = La, Nd$) ceramics. *Ceram. Int.* **2017**, *43*, 10861–10865. [[CrossRef](#)]
50. Toda, K.; Kurita, S.; Sato, M.; Toda, K.; Kuritab, S.; Satob, M. Synthesis and ionic conductivity of novel layered perovskite compounds, $AgLaTiO_4$ and $AgEuTiO_4$. *Solid State Ion.* **1995**, *81*, 267–271. [[CrossRef](#)]
51. Toda, K.; Kameo, Y.; Kurita, S.; Sato, M. Crystal structure determination and ionic conductivity of layered perovskite compounds $NaLnTiO_4$ ($Ln =$ rare earth). *J. Alloys Compd.* **1996**, *234*, 19–25. [[CrossRef](#)]
52. Singh, S.J.; Jayaram, R.V. Chemoselective O-tert-butoxycarbonylation of hydroxy compounds using $NaLaTiO_4$ as a heterogeneous and reusable catalyst. *Tetrahedron Lett.* **2008**, *49*, 4249–4251. [[CrossRef](#)]
53. Silyukov, O.I.; Abdulaeva, L.D.; Burovikhina, A.A.; Rodionov, I.A.; Zvereva, I.A. Phase transformations during $HLnTiO_4$ ($Ln = La, Nd$) thermolysis and photocatalytic activity of obtained compounds. *J. Solid State Chem.* **2015**, *226*, 101–106. [[CrossRef](#)]
54. Reddy, V.; Hwang, D.; Lee, J. Effect of Zr substitution for Ti in $KLaTiO_4$ for photocatalytic water splitting. *Catal. Lett.* **2003**, *90*, 39–44. [[CrossRef](#)]
55. Kawashima, K.; Hojamberdiev, M.; Chen, S.; Yubuta, K.; Wagata, H.; Domen, K.; Teshima, K. Understanding the effect of partial N^{3-} -to- O^{2-} substitution and H^+ -to- K^+ exchange on photocatalytic water reduction activity of Ruddlesden–Popper layered perovskite $KLaTiO_4$. *Mol. Catal.* **2017**, *432*, 250–258. [[CrossRef](#)]
56. Rodionov, I.A.; Silyukov, O.I.; Zvereva, I.A. Study of photocatalytic activity of layered oxides: $NaNdTiO_4$, $LiNdTiO_4$, and $HNdTiO_4$ titanates. *Russ. J. Gen. Chem.* **2012**, *82*, 635–638. [[CrossRef](#)]
57. Berdowski, P.A.; Blasse, G. Luminescence and energy migration in a two-dimensional system: $NaEuTiO_4$. *J. Lumin.* **1984**, *29*, 243–260. [[CrossRef](#)]

58. Ozawa, T.C.; Ikoshi, A.; Taniguchi, T.; Mizusaki, S.; Nagata, Y.; Noro, Y.; Samata, H.; Takayanagi, S. Low temperature magnetic properties of layered compounds: NaLnTiO_4 (Ln = Sm, Eu, Gd, Tb, Dy, Ho and Er). *J. Alloys Compd.* **2008**, *448*, 38–43. [[CrossRef](#)]
59. Ozawa, T.C.; Ikoshi, A.; Taniguchi, T.; Mizusaki, S.; Nagata, Y.; Noro, Y.; Samata, H.; Takayanagi, S. Magnetic spin interactions observed by heat capacity measurements for layered compounds: NaLnTiO_4 (Ln = Sm, Eu, Gd, Tb, Dy, Ho and Er). *J. Alloys Compd.* **2008**, *448*, 64–68. [[CrossRef](#)]
60. Tezuka, K.; Hinatsu, Y.; Preparation, S. Magnetic Properties of Layered Perovskites NaLnTiO_4 (Ln, Sm, Eu, and Gd). *J. Solid State Chem.* **1998**, *346*, 342–346. [[CrossRef](#)]
61. Silyukov, O.; Chislov, M.; Burovikhina, A.; Utkina, T.; Zvereva, I. Thermogravimetry study of ion exchange and hydration in layered oxide materials. *J. Therm. Anal. Calorim.* **2012**, *110*, 187–192. [[CrossRef](#)]
62. Zvereva, I.A.; Silyukov, O.I.; Chislov, M.V. Ion-exchange reactions in the structure of perovskite-like layered oxides: I. Protonation of NaNdTiO_4 complex oxide. *Russ. J. Gen. Chem.* **2011**, *81*, 1434–1441. [[CrossRef](#)]
63. Nishimoto, S.; Matsuda, M.; Harjo, S.; Hoshikawa, A.; Ishigaki, T.; Kamiyama, T.; Miyake, M. Neutron diffraction study on protonated and hydrated layered perovskite. *J. Solid State Chem.* **2006**, *179*, 3308–3313. [[CrossRef](#)]
64. Nishimoto, S.; Matsuda, M.; Harjo, S.; Hoshikawa, A.; Kamiyama, T.; Ishigaki, T.; Miyake, M. Structural change in a series of protonated layered perovskite compounds, HLnTiO_4 (Ln = La, Nd and Y). *J. Solid State Chem.* **2006**, *179*, 1892–1897. [[CrossRef](#)]
65. Abdulaeva, L.D.; Silyukov, O.I.; Petrov, Y.V.; Zvereva, I.A. Low-Temperature Transformations of Protonic Forms of Layered Complex Oxides HLnTiO_4 and $\text{H}_2\text{Ln}_2\text{Ti}_3\text{O}_{10}$ (Ln = La, Nd). *J. Nanomater.* **2013**, *2013*, 514781. [[CrossRef](#)]